Supporting Information

Discovery of a metastable van der Waals semiconductor via polymorphic crystallization of amorphous films

Yuta Saito*, Shogo Hatayama, Wen Hsin Chang, Naoya Okada, Toshifumi Irisawa, Fumihiko Uesugi, Masaki Takeguchi, Yuji Sutou, and Paul Fons

∗E-mail: yuta-saito@aist.go.jp

[Synthesis conditions]

Figure S1a shows the *R*–*T* curves for different temperature ranges, and the corresponding XRD results are shown in Figure S1b. The film remained in the amorphous phase until 220 °C and crystallized into a $GeTe_2$ phase, characterized by four strong XRD peaks [1]. The peak intensities continued to increase as the sample was heated to 240 °C, and then sharply decreased concomitantly with the appearance of peaks from the crystalline GeTe and Te phases above 250 °C. The abrupt change in the resistance corresponds to crystallization, that is, phase separation into GeTe+Te.

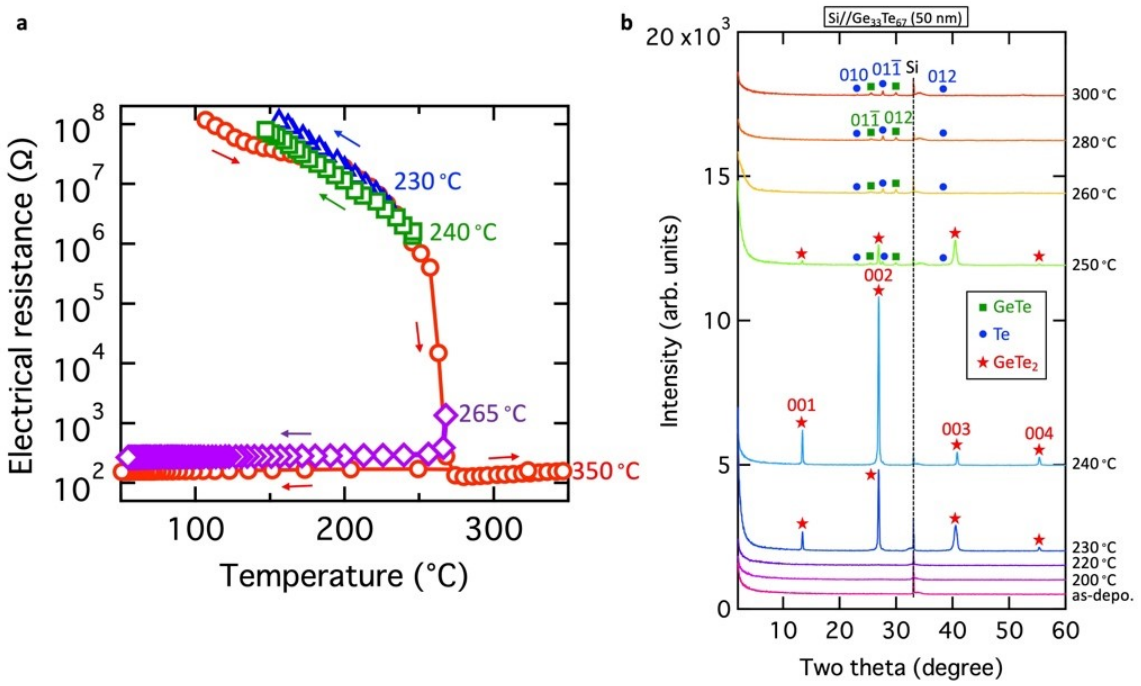

Figure S1. a) Temperature dependence of electrical resistance for different target temperatures. b) XRD patterns measured after annealing at different temperatures.

Stress may have a strong effect on the $GeTe_2$ crystallization process. Figure S2 shows a comparison of the out-of-plane XRD patterns for different sample conditions. Figure S2a shows a 5-nm-thick $Ge_{33}Te_{67}$ film grown on a Si substrate. The film remained in the amorphous phase even after annealing to 250 °C and showed low intensity; however, obvious peaks corresponding to the $GeTe_2$ phase appeared after annealing at 300 °C. This is consistent with the previous work by Tsunetomo et al., in that the transition temperature increases with decreasing film thickness. Although they only reported a minimum thickness of 62.5 nm [2]. In the current study, the trend was found to continue down to ultrathin films as thin as 5 nm. The trend of increasing crystallization temperature with decreasing film thickness is a general trend for many other phase-change materials [3].

An oxidation protection layer is important for chalcogenide materials, as surface oxidation can alter film properties [4,5]. The deposition of the protective layer prevented the formation of a pure $GeTe_2$ phase. Figure S2b shows the XRD results for a $Ge_{33}Te_{67}$ (10 nm) film covered with a 50-nm-thick SiO_2 layer grown subsequently in the same chamber. The film remained amorphous upon annealing at 250 °C; however, when the annealing temperature reached 260 °C, the XRD pattern showed a GeTe peak in addition to $GeTe_2$, suggesting the coexistence of two crystalline phases. Further heating to 280 °C resulted in the dominant phase being GeTe, with a tiny peak originating from $GeTe_2$. Therefore, it is necessary to carefully choose the cap layer material to avoid unwanted crystallization of the sample into GeTe. The deposition of the cap layer after the formation of the $GeTe_2$ phase is another possibility.

Next, XRD measurements were performed on a $Ge_{33}Te_{67}$ (50 nm) film grown on an Al_2O_3 single-crystal substrate. Annealing at 230 °C did not lead to crystallization, but when the temperature exceeded 235 °C, $GeTe_2$, GeTe, and Te peaks were present, as shown in Figure S2c. After annealing at 240 °C, the film was transformed into thermodynamically stable GeTe+Te phases with a trivial contribution from $GeTe_2$. This situation is strikingly different when the same film was grown on a SiO_2 glass substrate, followed by the same annealing conditions. Figure S2d clearly demonstrates that a single phase of $GeTe_2$ was formed with significantly sharper peak intensities in the temperature range of 235–250 °C. This result agrees well with the results obtained for a film grown on a Si substrate without a cap layer, as shown in Figure 2. As summarized in Figure S2, the effects of thickness, cap layer, and substrate on the formation of $GeTe_2$ suggests that internal stress plays a major role in addition to temperature. This can be intuitively understood as the formation of a metastable phase owing to changes in the free energy of the system induced by intensive variables. A quantitative

understanding of the formation process and corresponding thermodynamics of the metastable $GeTe_2$ phase is necessary to realize device applications.

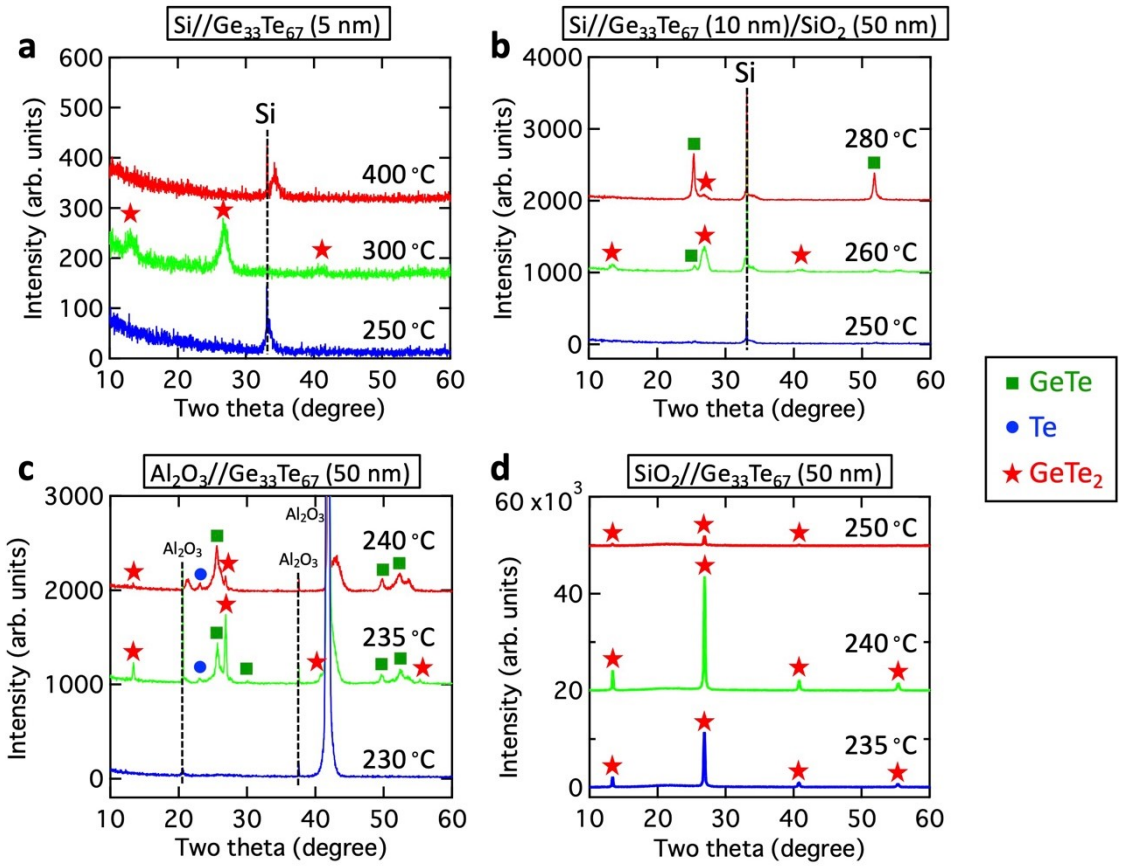

Figure S2. XRD patterns of a) 5-nm-thick $GeTe_2$ films, b) $GeTe_2$ films with a SiO_2 cap, c) $GeTe_2$ films on Al_2O_3 substrate, and d) $GeTe_2$ films on SiO_2 substrate.

The thermal stability of the metastable $GeTe_2$ phase was evaluated. After the formation of $GeTe_2$ phase, the sample was cooled down to room temperature and confirmed the single phase of $GeTe_2$ by XRD (Figure S3). Then, the same sample was heated again at 200 °C for 1h and 3h. Figure S3 shows that even after annealed for 3h at 200 °C, the XRD peak intensities are unchanged from the as-fabricated $GeTe_2$ phase, and furthermore, no additional peak from GeTe and Te appeared. This is remarkably higher than the amorphous-to-crystal transition temperatures of GeTe and $Ge_2Sb_2Te_5$, suggesting that the thermal stability of $GeTe_2$ is high enough for practical applications.

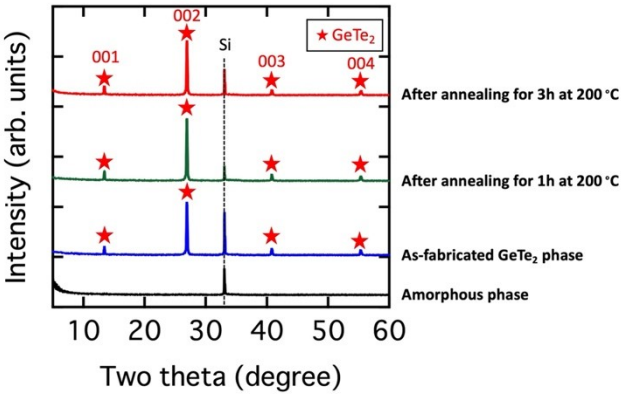

Figure S3. XRD patterns for $GeTe_2$ films after annealing at 200 °C for 1h and 3h.

[Determination of crystal structure]

In addition to the lattice constants obtained from the XRD analyses, there are other parameters necessary to determine the crystal structure, that is, the fractional coordinates of Te (x, y, z), if Ge is assigned as (0, 0, 0). Owing to the symmetry requirement of space group 164, the x and y coordinates are 1/3 and 2/3, respectively, while z is arbitrary. The z value affects the XRD peak intensity ratio. Figure S4 shows (a) our structural model for $GeTe_2$ and (b) the simulated relative peak intensities as functions of z. The normalized experimental peak intensities are also shown. The experimental XRD pattern for the $GeTe_2$ film showed that the 002 plane had the strongest intensity. With increasing z, a decrease and increase in the 001 and 003 peaks, respectively, was observed, as shown in Figure S4b. Although the current analytical procedure is only semi-quantitative, the value z=0.27 best explains the experimentally observed XRD pattern. A more detailed structural analysis is necessary to completely determine the structure of the metastable $GeTe_2$ phase; however, this is a challenging experiment because of the limitations in the sample volume. Therefore, in this study, we adapted the structural information shown in Figure 3(a), which well reproduces the experimental XRD patterns.

In addition to the above discussion, we argue that the 1T structure with space group 164 is a representative CdI_2-type structure [6]. CdI_2 is characterized as a hexagonal close-packed lattice with vdW gaps, in which Cd cations undergo octahedral coordination with iodine anions. Therefore, by analogy, Ge and Te are anticipated to correspond to Cd and I, respectively, in the case of $GeTe_2$. However, the chemical bonding of CdI_2 is strongly ionic because of the large electronegativity difference (Cd:1.69, I:2.66) versus $GeTe_2$ (Ge:2.01, Te:2.1) (all values are from the Pauling scale), suggesting that bonding in $GeTe_2$ has a more covalent character. Recently, the concept of metavalent bonding was proposed to describe bonding in Te-based chalcogenide materials [7]. We believe that the formation of metastable layered $GeTe_2$ is related to this type of unique bonding mechanism.

It should be noted that the structure was not relaxed before calculating the electronic structure. In fact, when the structure model was relaxed at 0 K in DFT, the lattice constants changed significantly to the extent that the XRD patterns could not be reproduced at all. This suggests that because $GeTe_2$ is a metastable phase, which can only be obtained via crystallization from the amorphous phase, other conditions must be satisfied for the metastable phase to form on computer. In other words, there must exist additional extensive thermodynamic parameters that result in a local potential minimum in the free energy that leads to the stabilization of the metastable phase. It is thought that stress can play such a role, according to the systematic investigation of XRD results under various fabrication conditions. Therefore, relaxation at 0 K without stress resulted in a different structure from that in the experiment, while structural relaxation under stress may improve the agreement.

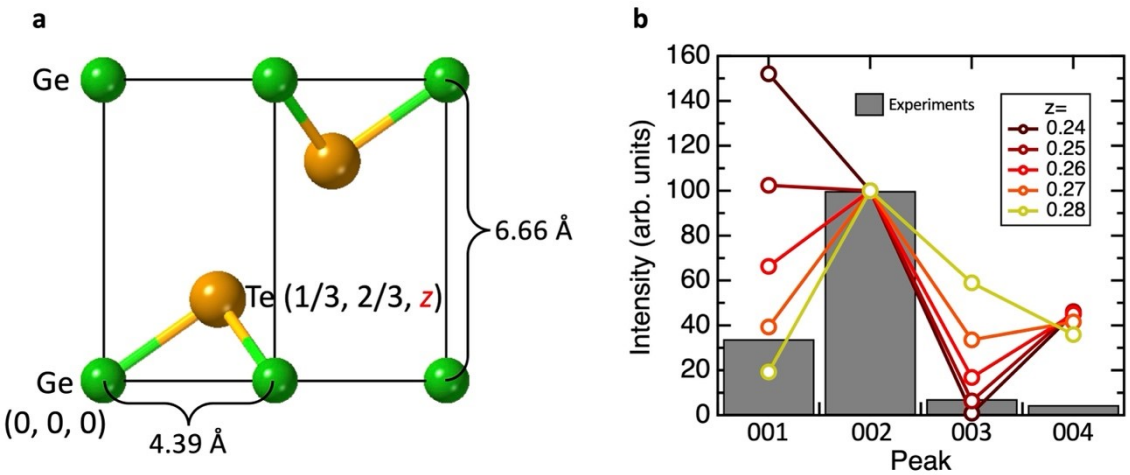

Figure S4. a) Unit cell of $GeTe_2$, where the *z*-coordinate of Te is a parameter. b) The *z*-dependence on XRD peak intensity ratio.

Table S1. Crystallographic data of $GeTe_2$ analyzed in this work.

Crystallographic data

Space Group	A	b	c	α	β	γ
P-3m1 (164)	4.39 Å	4.39 Å	6.66 Å	90°	90°	120°

Atom coordinates

Element	x	y	z
Ge	0	0	0
Te	0.33333	0.66667	0.27

Comparison of XRD peak positions (in degree)

Out-of-plane			In-plane		
Lattice plane	Simulation	Experiment	Lattice plane	Simulation	Experiment
001	13.29	13.30	010	23.38	23.32
002	26.77	26.80	110	41.09	41.10
003	40.64	40.65	020	47.81	47.86
004	55.16	55.20			

[Optical properties]

We have measured both transmittance (T) and reflectance (R) from the same $GeTe_2$ film grown on a SiO_2 glass substrate. The SiO_2 substrate was chosen as it is transparent and moreover, the metastable $GeTe_2$ phase was found to form with high quality as shown in Fig. S2d. Then, the absorption coefficient was calculated based on the following equation [8].

$$\alpha = \frac{1}{d}\ln\left\{\frac{(1-R)^2 + \left[(1-R)^4 + 4R^2T^2\right]^{1/2}}{2T}\right\},$$

where, d is the thickness of the film. Figure S5 shows measured T and R and calculated absorption coefficient.

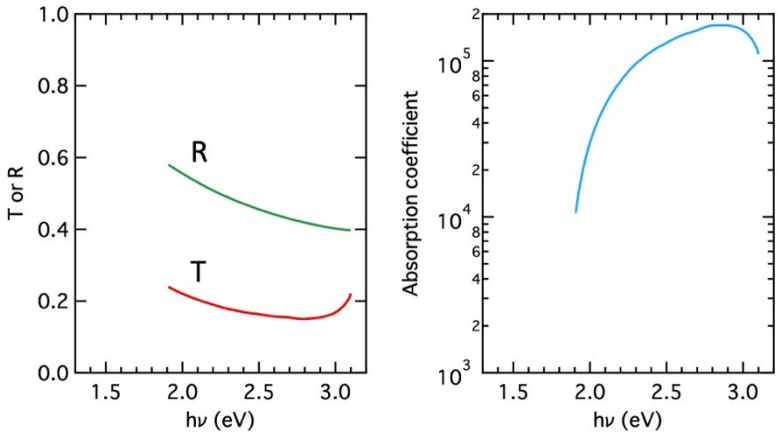

Figure S5 (Left) Measured transmittance (T) and reflectance (R) and (Right) calculated absorption coefficient.

[Electronic structure]

Note that the present calculation was performed for a perfect crystal without any defects, leading to a band structure with metallic features. If E_F is located inside the bandgap, the material exhibits semiconducting properties. Te vacancies, V_{Te}, or Ge antisite defects, Ge_{Te}, are possible donor impurities; thus, in the future, systematic DFT calculations on the formation energy for each defect are necessary. In fact, Malyi and Zunger recently reported that the standard DFT calculation of the band structure sometimes results in metallic behavior, while experiments reveal the presence of a band gap [9]. The authors described this situation as a case of a false metal and speculated that allowing for spontaneous defect formation may convert the false metal into an insulator. They used the example of Ba_4As_3, which shows a p-type degenerate gapped band structure, whereas the formation of donor vacancies (as in this case) results in the transfer of electrons from the donor level to the hole states in the valence band. The same analogy may apply to $GeTe_2$, where the formation of a spontaneous Te vacancy may

result in the filling of the hole states at the valence band maximum.

[Device]

Figure S6 shows XRD pattern of $GeTe_2$ film on the W bottom electrode. A single phase of $GeTe_2$ is confirmed on the W film, suggesting that the device measurements represent the physical properties of $GeTe_2$.

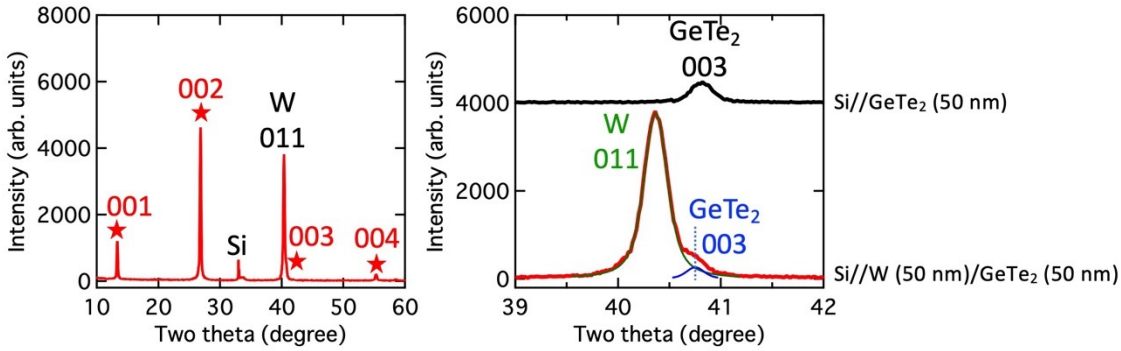

Figure S6. XRD pattern of $GeTe_2$ film on the W bottom electrode.

Figure S7 shows bipolar behavior of $GeTe_2$ vertical device.

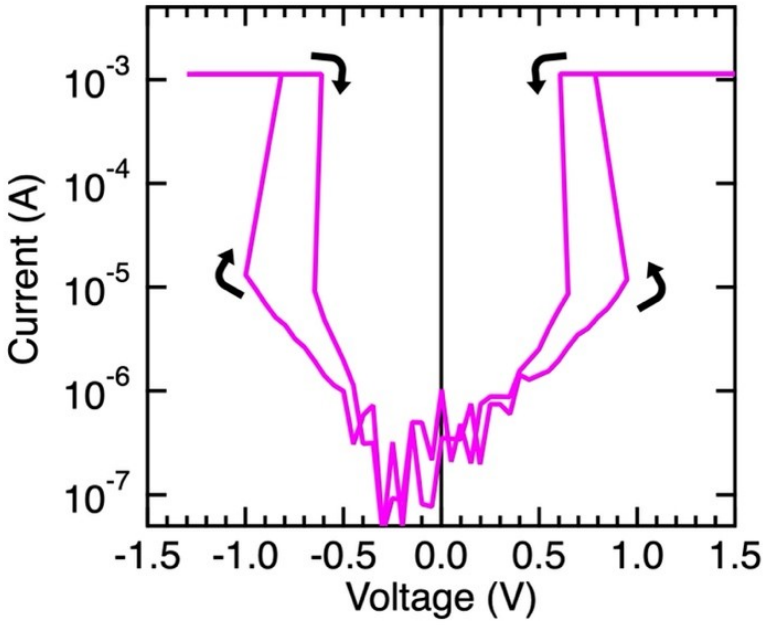

Figure S7. Bipolar *I–V* curve for $GeTe_2$ vertical device.

References

[1] Fukumoto, H., Tsunetomo, K., Imura, T., & Osaka, Y. Structural changes of amorphous

$GeTe_2$ films by annealing (formation of metastable crystalline $GeTe_2$ films). *Journal of the Physical Society of Japan* 56(1), 158–162. https://doi.org/10.1143/JPSJ.56.158 (1987).

[2] Tsunetomo, K., Sugishima, T., Imura, T., & Osaka, Y. Stability of metastable $GeTe_2$ in thin films. *Journal of Non-Crystalline Solids*, 95–96, 509–516. https://doi.org/10.1016/S0022-3093(87)80151-5 (1987).

[3] Raoux, S., Jordan-Sweet, J. L., & Kellock, A. J. Crystallization properties of ultrathin phase change films. *Journal of Applied Physics* 103(11), 114310. https://doi.org/10.1063/1.2938076 (2008).

[4] Saito, Y., Sutou, Y., & Koike, J. Fast crystal nucleation induced by surface oxidation in Si-doped GeTe amorphous thin film. Applied Physics Letters 100(23), 231606. https://doi.org/10.1063/1.4726107 (2012).

[5] Agati, M., Gay, C., Benoit, D., & Claverie, A. Effects of surface oxidation on the crystallization characteristics of Ge-rich Ge-Sb-Te alloys thin films. *Applied Surface Science* 518, 146227. https://doi.org/10.1016/j.apsusc.2020.146227 (2020).

[6] Bozorth, R. M. The crystal structure of cadmium iodide. *Journal of the American Chemical Society* 44(10), 2232–2236. https://doi.org/10.1021/ja01431a019 (1922).

[7] Wuttig, M., Deringer, V. L., Gonze, X., Bichara, C., & Raty, J.-Y. Incipient metals: functional materials with a unique bonding mechanism. *Advanced Materials* 30(51), 1803777. https://doi.org/10.1002/adma.201803777 (2018).

[8] Vahalová, R., Tichý, L., Vlcek, M., & Tichá, H. Far Infrared Spectra and Bonding Arrangement in Some Ge–Sb–S Glasses. *Phys. Stat. Sol. (a)* 181, 199-209 (2000).

[9] Malyi, O. I. & Zunger, A. False metals, real insulators, and degenerate gapped metals. *Applied Physics Reviews* 7(4), 041310. https://doi.org/10.1063/5.0015322 (2020).